Cover Page

1) Title of the paper:

Cerebral Artery Classification: Integrating Synthetic Models with MRA Data

2) authors' affiliation and address:

LTeN, UMR-6607, Polytech' Nantes, France

&

INSERM, UMR-1087, l'institut du thorax, Nantes, France.

3) e_mail address:

Florent.Autrusseau@univ-nantes.fr

4) Conference & Publisher information:

https://embc.embs.org/2025/

5) bibtex entry:

```
@InProceedings{EMBC25_TopCoW,
  author    = {N. Mansouri and V. {L'Allinec} and R. Bourcier and F. Autrusseau},
  booktitle = {47th Intl. Conf. of the IEEE Engineering in Medicine and Biology Society (EMBC) },
  date      = {2025-07-14},
  title     = {Cerebral Artery Classification: Integrating Synthetic Models with MRA Data},
}
```

Cerebral Artery Classification: Integrating Synthetic Models with MRA Data

Nesrin Mansouri[1], Vincent L'Allinec[1,2], Romain Bourcier[1,3] and Florent Autrusseau[1,4]

***Abstract*— The Circle of Willis (CoW) plays a critical role in cerebral vascular circulation, yet its high anatomical variability complicates accurate segmentation and artery classification, particularly in clinical settings. While Magnetic Resonance Angiography (MRA) images are commonly used for segmentation, the scarcity of comprehensive, annotated datasets limits the performance of machine learning models. In this study, we leverage synthetic models generated by VaMos, a vascular modeling tool, to augment the existing TopCoW dataset. By incorporating these anatomically plausible synthetic structures alongside actual MRA data, we improve artery classification using a deep learning model, specifically nnUNet, which is optimized for medical image segmentation. For smaller/thinner and underrepresented arteries, such as the posterior and anterior communicating arteries, the improvement was around 16%. This approach provides a novel solution to data scarcity, showing that synthetic models can effectively complement real data to improve segmentation performance in challenging anatomical regions.**

I. INTRODUCTION

The Circle of Willis (CoW) is a ring of arteries located at the base of the brain, primarily responsible for ensuring continuous blood flow to the brain by providing collateral circulation between the brain's anterior and posterior regions [1], [2]. Its main role is to compensate for any blockages or disruptions in blood flow to maintain adequate oxygen supply. Studies have shown that approximately 50-60% of people have anatomical variations or an incomplete CoW, which can reduce its effectiveness in fulfilling this compensatory function [3], [4]. Recent studies [5], [6] provide examples of the different variants of the CoW, illustrating the diverse forms these structures can take and their potential impact on cerebral circulation. These variations can increase the risk of ischemic events, particularly in cases of arterial blockage or stenosis [7], [8], [9]. Moreover, the diameter of collateral vessels plays a critical role in its capacity to maintain the blood flow. While arteries with diameters under 1 mm were previously considered hypoplastic [10] recent studies suggest that the functional threshold for effective cross-flow through the anterior and posterior communicating arteries is between 0.4 and 0.6 mm, highlighting that even smaller arteries can contribute to collateral circulation under certain circumstances [11], [12].

*This work was supported by the RHU-ANR project "eCAN" #ANR-23-RHUS-0013.

[1]N. Mansouri is with the Institut du Thorax (ITX), Univ. of Nantes, France. [1,2]V. L'Allinec is with the ITX, Univ. of Nantes, and Univ. hospital, Angers, France. [1,3]R. Bourcier is with the Univ. Hospital in Nantes and ITX, Nantes, France. [1,4]F. Autrusseau is with the ITX and LTeN, Univ. of Nantes, France. <FirstName>.<LastName>@univ-nantes.fr

Accurately classifying the arteries of the CoW is crucial not only for understanding its complex angio-architecture but also for identifying pathological conditions like intracranial aneurysms (IAs). IAs often form in regions of vascular weakness or abnormality and can lead to life-threatening complications such as hemorrhagic strokes [13]. By classifying CoW arteries, we gain key insights into the mechanisms behind IA development and the diverse shapes these aneurysms can take [14], [15]. Variations in aneurysm shape are influenced by hemodynamic stress and structural anomalies, particularly onto bifurcations, where the risk of IA formation is higher. Moreover, aneurysm characteristics like shape irregularities (e.g., blebs) and changes in size are critical rupture risk factors. Understanding these features is essential for predicting rupture risk and guiding targeted therapeutic interventions. Given the critical role of anatomical and hemodynamic factors in IAs formation, accurate artery classification in the CoW is essential for identifying high-risk areas, particularly onto the bifurcations.

However, despite its clinical relevance, characterizing the CoW is challenging due to both clinical and technical factors. Clinically, its complex and highly variable anatomy demands expert interpretation for accurate assessment. Technically, the variability in imaging data—stemming from different modalities, resolutions, and patient-specific factors—further complicates the development of reliable and consistent analysis methods. These challenges underscore the growing need for efficient tools that can accurately analyze and compare the angio-architecture of the cerebral vascular tree, ultimately improving the efficiency and precision of CoW assessments.

The CoW is primarily imaged using either Magnetic Resonance Angiography or Computed Tomography Angiography (CTA). However, publicly available datasets for CoW imaging are limited, with MRA datasets often lacking sufficient annotations and CTA datasets being even rarer. To overcome these limitations, the TopCoW challenge[1] released a joint-modal dataset (CTA and MRA) with accurate annotations, challenging the community to improve CoW characterization and segmentation in medical imaging [16].

To enhance dataset availability and overcome limitations of annotated data, we incorporated synthetic models of CoW arteries generated by the Vascular Models (VaMos)[2] tool [17], which simulates geometric features of arterial bifurcations and surrounding structures. These synthetic models allowed us to augment the dataset, improving the general-

[1]https://topcow24.grand-challenge.org/

[2]https://gitlab.univ-nantes.fr/autrusseau-f/vamos

ization of machine learning models for artery classification. However, since VaMos is currently designed to mimic MRA Time-of-Flight (ToF) acquisitions, only MRA data was considered in this study.

Synthetic data generation has proven effective in improving segmentation performance, as demonstrated in [18], though prior methods mainly focused on variations of existing data. VaMos offers a novel approach by generating anatomically accurate vascular models, incorporating key features like diameter, tortuosity, and bifurcation geometry, closely mirroring real-world conditions. In an approach similar to the work carried out in [19] on brain tumor segmentation, we have extended the use of synthetic data to cerebral vascular trees, addressing the unique challenges of CoW segmentation. Deep learning models like nnUNet [20] have been widely applied in vascular segmentation tasks, showing significant promise. By integrating synthetic models with real MRA data via an nnUNet, our aim is to improve segmentation accuracy and robustness.

In this study, a nnUNet was applied for multiclass segmentation of the CoW using the TopCoW dataset and we evaluated the impact of incorporating synthetic models from VaMos. Our hybrid approach aims to improve artery classification performance by leveraging both real and synthetic data to enhance segmentation accuracy.

II. Material & Methods

A. Dataset Description and Annotation Protocol from the TopCoW Challenge

In this study, we utilize the MRA images provided by the TopCoW challenge dataset. The dataset consists of patients admitted to the Stroke Center at the University Hospital Zurich (USZ) between 2018 and 2019. Inclusion criteria required that both MRA and CTA scans be available for each patient, with at least one of the modalities allowing for the assessment of the CoW anatomy. The patients in this cohort were diagnosed with or recovering from stroke-related neurological disorders, including ischemic stroke, transient ischemic attack, retinal infarct, intracerebral hemorrhage, and cerebral sinus vein thrombosis.

The MRA data were acquired using various Siemens scanners, with magnetic field strengths of either 3 Tesla or 1.5 Tesla, following standard clinical protocols. Most data were collected at USZ, with some cases from neighboring Swiss hospitals. The data is multi-site, representing scans from different locations in Switzerland. To ensure patient privacy, the data were anonymized, and additional defacing and cropping procedures were applied to focus solely on the braincase region. The MRA images were converted from DICOM to NIfTI format, and defacing was performed using the quickshear method to remove facial regions [21].

Virtual Reality (VR) was used to efficiently annotate and verify the CoW anatomy in 3D, enabling the creation of voxel-level multiclass segmentation masks for each MRA image [22]. These masks labeled 13 arteries of the CoW, including the Internal Carotid Arteries (ICA), Anterior Cerebral Arteries (ACA), Middle Cerebral Arteries (MCA), Anterior communicating artery (Acom), Posterior communicating arteries (Pcom), Posterior Cerebral Arteries (PCA), Basilar Artery (BA), and, in some cases, a third A2 artery (3rd A2). Figure 1a shows the fully annotated CoW, while Figure 1b presents a zoomed-in view of the CoW, highlighting the detailed segmentation of the 13 arteries. Note that only vessel components and regions essential for diagnosing the CoW angio-architecture and its variants were annotated.

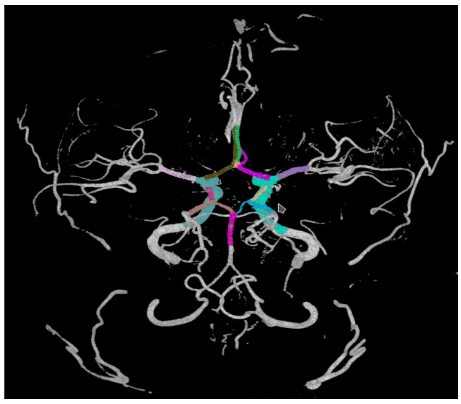

(a) Annotated Circle of Willis (CoW).

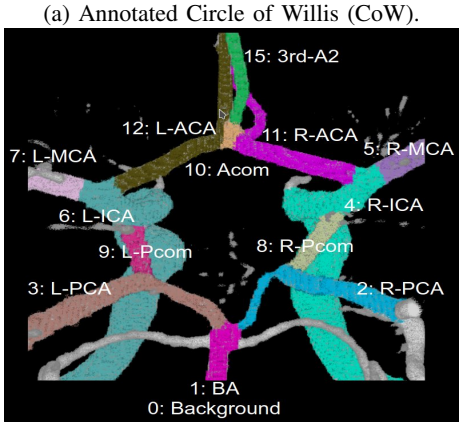

(b) Zoomed-in view showing the 13 arteries.

Fig. 1: Visualization of the annotated data: (a) Full Circle of Willis with labeled vessel components, and (b) zoomed-in view highlighting the 13 key arteries [16].

B. Methodology: Three-Step Approach for Circle of Willis Artery Segmentation

In this study, we introduce a three-step approach to accurately segment and classify the arteries of the CoW in MRA-ToF images. A schematic diagram of these steps is presented in Figure 2, and the following sections provide a detailed explanation of each step:

1) Step 1 - Vascular Tree Segmentation: In the first step of our approach, we focus on segmenting the vascular system through the training of a nnUNet model. The primary objective of this step is to effectively isolate and delineate the vascular structures, which will form the foundation for subsequent analysis. This segmentation process aims to remove irrelevant areas, ensuring that only essential vascular regions are retained. In doing so, we isolate the vascular

tree, which will facilitate the identification of the region of interest (ROI) at later stages of the pipeline. The specifics of the training procedure, the methodology for data splitting, and the model parameters are detailed in section II-D.

For this step, we utilized a dataset distinct from the one provided by the TopCoW challenge. We employed 175 MRA images collected from over thirty French institutions. Detailed information about this dataset can be found in [17]. The images were annotated by a trained operator (author F.A.), and validated by a neuroradiologist with 10 years of experience (author R.B.). The labels are 0 for background and 1 for the vascular tree.

2) Step 2 - ROI Extraction: Following the vascular tree segmentation, the second step involves extracting the ROI, which encompasses all arteries composing the CoW. Initially, small, disconnected components are removed. We then calculate the center of mass (COM) for the remaining components. Based on the COM and prior anatomical knowledge, a bounding box is created with dimensions set to 40% of the original size in the x-direction, 30% in the y-direction, and 35% in the z-direction. This bounding box is used to crop both the ToF images and their corresponding labels. In the third step, which is crucial for achieving our objective, we employ the VaMos framework to generate synthetic data from the cropped ToF images, thereby augmenting the dataset and increasing the diversity of training examples. VaMos will primarily be applied to cases that include arteries less represented in the database, helping to better capture and enhance the representation of these arteries (which may be missing in some individuals).

3) Step 3 - CoW Artery Classification: In the third step, both the original MRA images and the newly generated synthetic images are augmented and then fed into a nnUNet model. The goal is to train the model to accurately segment the 13 arteries composing the CoW. This process involves data splitting, training, and testing, and the used model parameters are consistent with those applied in the nnUNet model from step 1. A detailed explanation of the data splitting procedure, training and testing protocols, and model configuration will be provided in section II-D.

C. Synthetic modeling using VaMos (Vascular Models)

In previous works [17], [23], we have introduced synthetic vascular models using the VaMos Software to generate realistic vascular structures for medical imaging applications.

In this study, to augment our dataset, we applied VaMos to the 125 MRA images from the TopCoW challenge. For each original MRA image, we generated multiple synthetic models by varying two key parameters:

1) Artery Diameter: We applied a random modification between -10% and +10% of the original artery diameter to simulate natural variations.
2) Artery Tortuosity: We introduced random spline modifications by adjusting the spline coefficients, effectively altering the arterial tortuosity. This was achieved by modifying the B-Splines' coefficients, which define the smoothness and curvature of the arteries' centerlines.

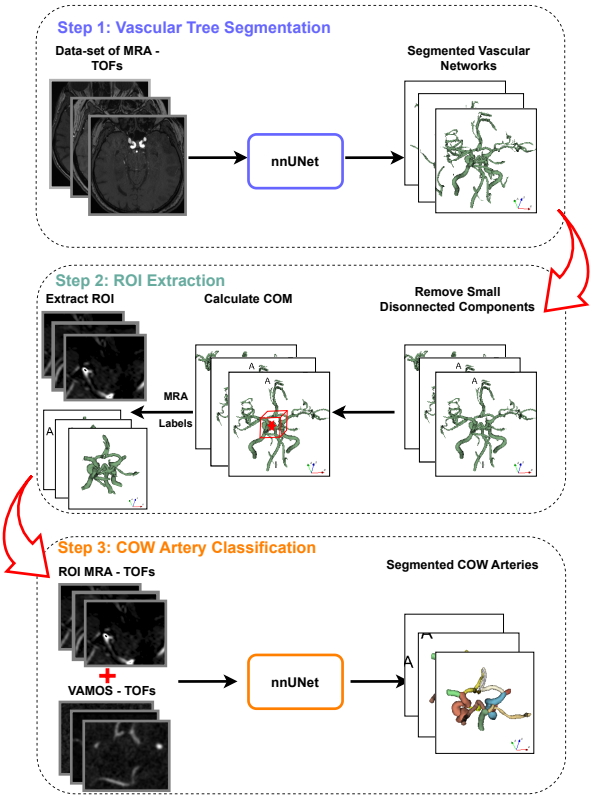

Fig. 2: Schematic of the three-step approach for CoW arteries classification: 1) vascular network segmentation (via nnUNet), 2) Region of Interest extraction, 3) synthetic data generation (VaMos) to enhance artery classification.

Other parameters are inherently randomized within VaMos, such as the background noise shape and standard deviation, or the vacular tree contrast and its radio-opacity.

These modifications enabled the creation of 495 synthetic vascular images, thus greatly enhancing the diversity of our dataset. Notably, VaMos was applied to cases containing arteries less represented in the database, such as the two posterior communicating arteries as well as the third A2 artery, to increase their representation and ensure a comprehensive coverage of the vascular structures.

D. Data Splitting and Model Setup

1) Data Splitting: In this study, we divided the dataset into training and testing subsets, as illustrated in Fig. 3. For training, both the original and synthetic MRA images were used, while the testing subset, comprising 15% of the total dataset, included 18 cases selected exclusively from the original MRA images. This approach aimed to evaluate the model performance on unseen real data, ensuring its ability to generalize to new, real-world scenarios. The training data underwent a 5-fold cross-validation with random assignment, thus ensuring that each data point was used for both training and validation across different iterations. Once trained, the model was tested on the designated test data.

The 18 test cases were selected to represent the full data

Arteries	Orig. data (%)	Orig + Synth. data (%)
BA	100	100
R-PCA	100	100
L-PCA	100	100
R-ICA	100	100
R-MCA	98.4	94.35
L-ICA	100	100
L-MCA	100	100
R-Pcom	48.8	**61.13**
L-Pcom	44.8	**54.68**
Acom	84.8	82.9
R-ACA	100	100
L-ACA	100	100
3rd-A	12.8	**32.26**

TABLE I: Percentage of occurrence of each CoW artery across the original TopCoW dataset and the augmented dataset including synthetic data (bold figures represent the most significant occurrence increase).

set, paying particular attention to the presence and absence of various arteries. Overall, out of the 18 test cases, the R-Pcom was missing in 8 ToF acquisitions, the L-Pcom was missing in 10 ToF, the Acom was missing in 6 images and finally, for 13 cases out of 18, the 3rd-A2 was missing. These variations in artery presence reflect a wide range of anatomical differences, allowing for a comprehensive assessment of the model's performance across different artery configurations.

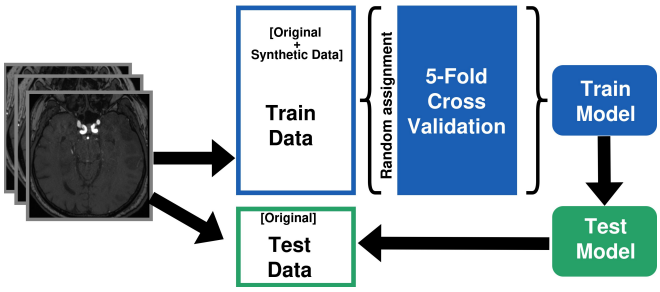

Fig. 3: Schematic of data splitting and 5-fold cross-validation, with 602 training cases (original and synthetic) and 18 test cases.

2) Model Setup:

Preprocessing

To ensure consistent voxel spacing across all images, we retrieved the original voxel spacing and size, then set the output spacing to be uniform in all three dimensions ($0.4 \times 0.4 \times 0.4$ mm). Nearest neighbor interpolation was used for label images to preserve the labels, while linear interpolation was applied to regular images. This resampling process was essential to maintain uniformity in the MRA images used to train the nnUNet model.

Training Configuration

Loss Function: We utilized the default loss function in nnUNet, which is weighted cross-entropy loss for the multi-class segmentation task. Epochs and Validation: The model was trained for 1,000 epochs with 5-fold cross-validation to ensure robust evaluation.

Postprocessing

Connected Component Analysis: We employed the default post-processing provided by nnUNet, which includes connected component analysis to filter out small connected components. We did not set a specific threshold for the largest connected component, as we relied on the default settings.

Computational Resources

Hardware: Training was conducted on a local machine equipped with an NVIDIA RTX A6000 GPU (49,140 MiB total memory) and an Intel Xeon W-3433 CPU (16 cores, 2 threads per core, 4,200 MHz max clock speed).

Model Architecture

Convolutional Layers: The model utilized standard convolutional layers. The background class (index 0) was included during training, and the evaluation metrics (e.g., Dice score, Recall and Precision) took the background into account.

III. Results

The first result, presented in Table I, shows how the use of synthetic images alongside the ground truth acquisitions can notably harmonize the training dataset. Before applying VaMos, the presence of the L-Pcom & R-Pcom and 3rd-A2 arteries in the dataset was 48.8%, 44.8%, and 12.8%, respectively. After applying VaMos, these percentages increased to 61.13% for L-Pcom, 54.68% for R-Pcom, and 32.26% for 3rd-A2. We can hence observe the ability of VaMos to multiply underrepresented arteries, particularly the 3rd-A2 artery, which showed the most significant increase. Additionally, VaMos increased the database size by generating synthetic vascular structures, with the data being close to real anatomical variations. We did not generate additional synthetic arteries for less represented arteries like the 3rd-A2, L-Pcom, and R-Pcom because only four cases in the dataset contain all these arteries. Relying solely on these four cases to expand the database would result in limited variability and increase the risk of overfitting, as the model would be trained on a narrow set of anatomical structures, limiting its ability to generalize effectively to new and unseen data. This extension of the dataset is crucial for improving model learning, as it enables improved generalization without introducing unrealistic data, thus contributing to better segmentation performance, particularly for under-represented arteries such as the 3rd-A2.

Fig. 4, shows a comparison between a Ground Truth (GT) crop and various modeled images. The left panel represents the original data (MRA ToF and its corresponding Segmented label), while the right panel shows three different synthetic images generated by VaMos. As can be observed, the geometrical configuration of the vascular structures is effectively modeled, closely mimicking the ToF images. Subtle diameter and tortuosity modifications in the modeled bifurcations are accurately captured, showcasing the model's ability to reproduce fine anatomical details with high fidelity.

During the TopCoW challenge, the 13 CoW arteries were divided into two groups to better evaluate model perfor-

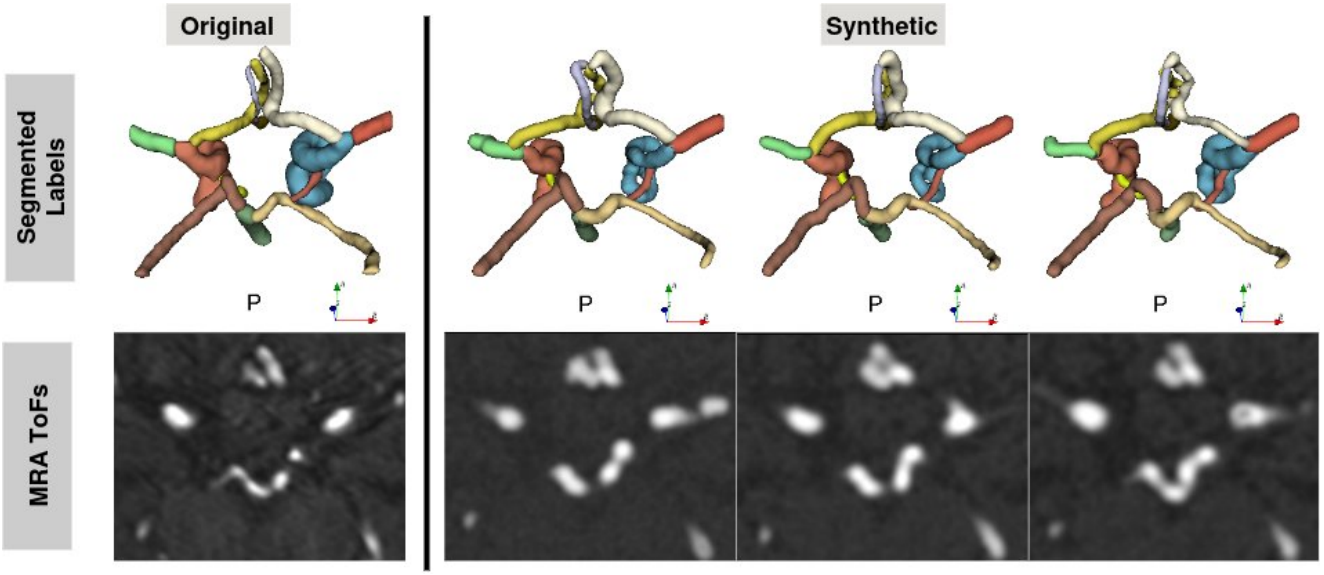

Fig. 4: Example of the original MRA image from the TopCoW Challenge (top row) and five VaMos-generated images (bottom row), with modifications in artery angle, tortuosity, and diameter.

mance. Group 1 includes non-communicating arteries that are almost always present, such as the basilar artery, posterior cerebral arteries, internal carotid arteries, middle cerebral arteries, and anterior cerebral arteries which are generally larger and easier to segment. Group 2 consists of the more variable, smaller, thinner communicating arteries, such as the L-Pcom, R-Pcom, Acom, and 3rd-A2 arteries, which are more challenging to segment. We will follow this division to better assess the results, allowing for a clearer evaluation of the model's performance on different artery types and the impact of synthetic data augmentation.

Table II presents a comparison of the overall performance between the original dataset and the augmented dataset (original + synthetic data), with metrics averaged across 13 classes, as well as for Group 1 and Group 2 arteries, during the test phase. Key evaluation metrics—Dice, Precision, and Recall—are reported for each artery class.

On the test set, when trained solely on the original dataset, the overall average Dice score was 77.88, with Precision at 78.25 and Recall at 86.45 (Table II). However, performance varied significantly among artery groups. For Group 1 arteries, which include the larger and more prominent arteries, the Dice score was 87.73, while for Group 2, which comprises smaller and more complex arteries, the Dice score dropped to 55.72. Notably, the challenging Group 2 arteries, such as the R-Pcom, L-Pcom and the 3rd A2 arteries, exhibited lower performance. This indicates that certain artery classes were more difficult to segment with the original dataset alone, likely due to their smaller size and anatomical complexity.

In contrast, when VaMos-generated synthetic data are incorporated into the training set, there is a significant improvement in segmentation performance across all artery groups. The overall average Dice score increases to 83.72, with Precision and Recall improving to 83.09 and 88.7, respectively (Table II). Notable improvements are observed in the previously challenging Group 2 arteries, where the Dice score rises from 55.72 to 68.035. Similarly, Group 1 arteries also see a boost, with Dice scores increasing from 87.73 to 90.70. These results demonstrate that synthetic data not only improved the performance for smaller and more complex arteries but also enhanced the segmentation accuracy for larger arteries, contributing to overall improved robustness of the model.

The inclusion of synthetic data from VaMos has thus proved to be highly beneficial, improving both the quality and consistency of segmentation, particularly for underrepresented or difficult-to-segment artery classes. By augmenting the dataset with synthetic models that mimic the geometric features of the CoW arteries, the model has gained more comprehensive training data, which has led to better generalization and higher accuracy in the segmentation task.

Metric	Dice	Recall	Precision
All (Orig)	77.88	78.52	86.45
All (Orig + Synth)	83.72	83.09	88.7
Group1 (Orig)	87.73	87.15	89.20
Group1 (Orig + Synth)	90.70	89.25	92.55
Group2 (Orig)	55.72	59.1	80.26
Group2 (Orig + Synth)	68.035	69.23	80.04

TABLE II: Performance comparison for original data (Orig) and augmented data (Orig + Synth) on the average of all arteries, Group 1 and Group 2 arteries on the test data-set.

The overall performance improvements highlighted earlier, especially the increase in Dice score from 77.88 to 83.72 when using synthetic data, are consistently reflected across different artery classes. To further understand the impact of these improvements, we break down the results by individual arteries, demonstrating how both large and small arteries benefited from the inclusion of synthetic data.

Breaking down the results per artery on the validation set,

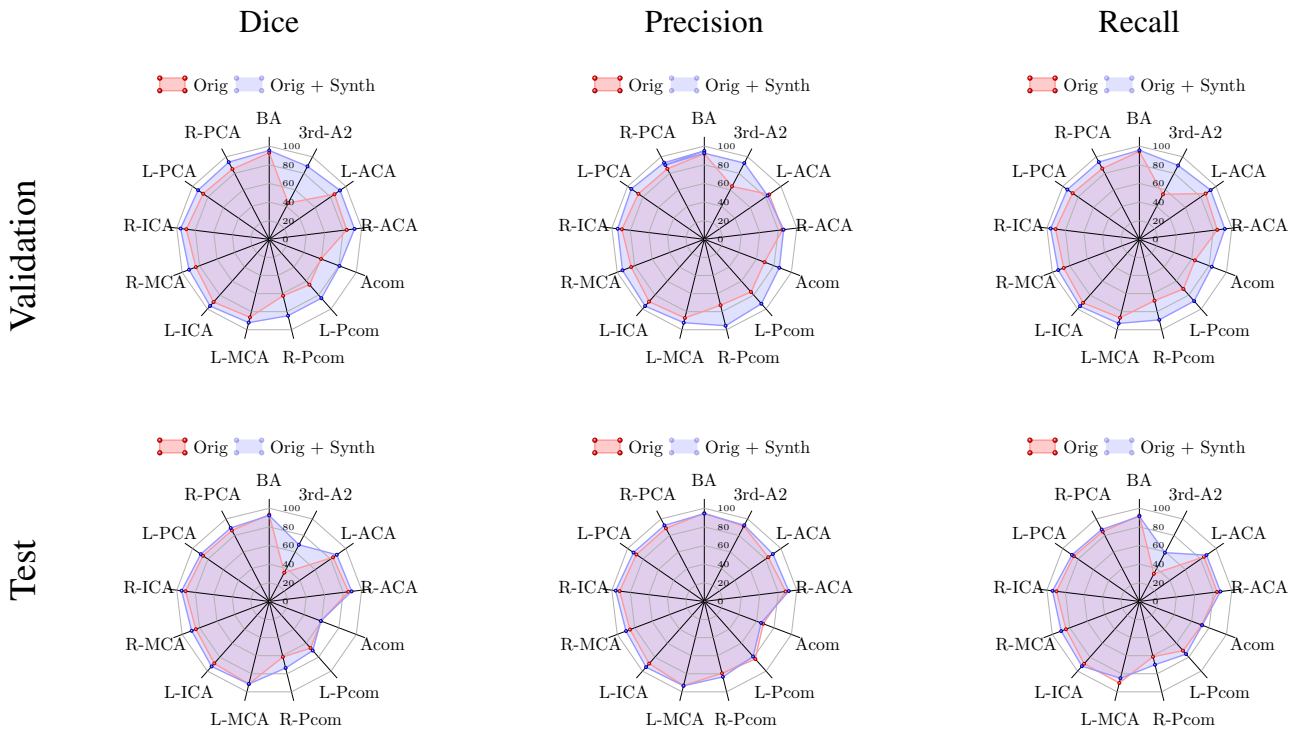

Fig. 5: Multiclass segmentation results on the validation set for all 13 CoW artery classes in terms of Dice, Recall, and Precision. The red line shows the performance when trained solely on the original data, while the blue line incorporates both original and synthetic data.

we observe that large arteries such as the R-ICA and L-ICA already performed well on the original dataset, achieving Dice scores of 89.63 for R-ICA and 90.09 for L-ICA (Fig. 5). However, segmentation of smaller arteries like the L-Pcom, R-Pcom and 3rd A2 arteries was more challenging, with Dice scores of 62.44 for L-Pcom 65.19 for R-Pcom, and 43.96 for 3rd-A. With the addition of synthetic data, these challenging arteries exhibited substantial improvement, with L-Pcom's Dice score rising to 84.54, R-Pcom 84.46 and 3rd-A to 88.46. The larger arteries also maintained their high performance, further validating the efficacy of synthetic data in enhancing segmentation accuracy.

Similarly, the benefits of synthetic data were evident on the test set. Larger arteries, such as the R-ICA and L-ICA, saw Dice score improvements from 90.53 to 94.77 and 88.95 to 93.36, respectively. Smaller and more complex arteries, like the R-Pcom, showed an increase from 61.44 to 73.68, the L-Pcom from 67.01 to 70.5, and the 3rd A2 from 34.81 to 68.67. This comprehensive improvement across both validation and test sets underscores the effectiveness of synthetic data in addressing variability in segmentation performance, especially for smaller and anatomically more complex arteries.

These findings confirm the model's robustness and show a significant performance improvement across most artery classes, with synthetic data playing a key role in enhancing segmentation accuracy on unseen data.

The example test case in Figure 6 shows the original MRA image (left) and the corresponding model prediction (right) using the hybrid approach combining synthetic and original data for artery segmentation in the CoW. Both the L-Pcom and R-Pcom arteries exhibited varying diameters and were extremely thin, making accurate prediction challenging. Despite these difficulties, our model was able to predict even the tiniest arteries, capturing subtle differences between the predicted and original images. As observed, while there is a small discrepancy in the left Pcom, the model still managed to effectively segment these challenging, thin arteries, highlighting its strength in dealing with intricate vascular details.

IV. Discussion & Conclusion

In this study, we addressed the challenge of segmenting underrepresented and anatomically complex arteries in the Circle of Willis by integrating synthetic vascular models with actual MRA data. The results clearly demonstrate the effectiveness of incorporating synthetic data into the training process, particularly for smaller arteries such as the posterior communicating arteries and the rare third artery. Prior to augmentation, these arteries exhibited suboptimal segmentation performance due to their size and anatomical complexity. After including synthetic data, segmentation accuracy for these arteries improved significantly, with Dice scores rising by over 34% for the 3rd-A, by approximately 12% for the R-Pcom arteries and by 4% for the L-Pcom.

Moreover, the overall performance of the model saw a substantial boost. The average Dice score increased from

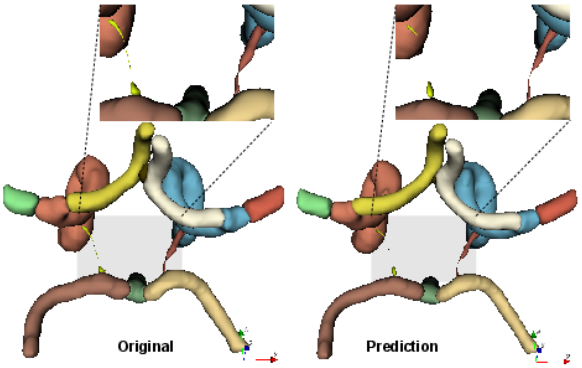

Fig. 6: Example test case showing the original MRA image (left) and the corresponding model prediction (right) using a hybrid approach that combines synthetic and original data for artery segmentation in the Circle of Willis.

77.88% to 83.72% on the test set, with Recall improving from 78.52% to 83.09% and Precision rising from 86.45% to 88.7%. These improvements were not only restricted to difficult-to-segment arteries but were observed across both larger and more complex arteries. This reinforces the contribution of synthetic data in enhancing segmentation accuracy and generalizing the model to better handle anatomical variability across the full spectrum of arteries in the CoW.

Our approach builds upon earlier studies that have highlighted the importance of data augmentation in medical image segmentation, particularly for structures with high anatomical variability, such as the CoW While previous efforts have focused on improving segmentation using real MRA or CTA data, the scarcity of comprehensive, annotated datasets has remained a limitation [16]. By introducing VaMos-generated synthetic vascular structures, we provide a novel solution that not only expands the training dataset but also enhances segmentation performance without compromising anatomical fidelity. This addresses the gap highlighted by studies that emphasize the need for more representative and diverse training data in CoW segmentation tasks [3], [4]. Future work may explore the use of additional imaging modalities and advanced techniques like adversarial training to tackle more extreme anatomical variations. These advancements could further refine segmentation performance and broaden the applicability of synthetic data augmentation approaches in medical imaging.

Lastly, although our study focused on the CoW the synthetic modeling approach developed here could be generalized to other vascular networks or anatomical structures. Future work could investigate the applicability of VaMos to other medical imaging challenges, expanding the scope of synthetic data augmentation in healthcare.

References

[1] O. AG, "Osborn's brain: imaging, pathology, and anatomy," *Salt Lake City, Utah: Amirsys*, 2013.

[2] T. Willis, *Cerebri anatome: cui accessit. Nervorum descriptio et usus*. Apud Gerbrandum Schagen, 1973, vol. 1.

[3] M. J. Krabbe-Hartkamp, J. Van der Grond, F. De Leeuw, J. De Groot, A. Algra, B. Hillen, M. Breteler, and W. Mali, "Circle of willis: morphologic variation on three-dimensional time-of-flight mr angiograms." *Radiology*, vol. 207, no. 1, pp. 103–111, 1998.

[4] S. Iqbal, "A comprehensive study of the anatomical variations of the circle of willis in adult human brains," *Journal of clinical and diagnostic research: JCDR*, vol. 7, no. 11, p. 2423, 2013.

[5] L. B. Hindenes, A. K. Håberg, L. H. Johnsen, E. B. Mathiesen, D. Robben, and T. R. Vangberg, "Variations in the circle of willis in a large population sample using 3d tof angiography: The tromsø study," *PLoS One*, vol. 15, no. 11, p. e0241373, 2020.

[6] B. Forgo, A. D. Tarnoki, D. L. Tarnoki, *et al.*, "Are the variants of the circle of willis determined by genetic or environmental factors? results of a twin study and review of the literature," *Twin Research and Human Genetics*, vol. 21, no. 5, pp. 384–393, 2018.

[7] B. J. Alpers, R. G. Berry, and R. M. Paddison, "Anatomical studies of the circle of willis in normal brain," *AMA Archives of Neurology & Psychiatry*, vol. 81, no. 4, pp. 409–418, 1959.

[8] K. Kapoor, B. Singh, and I. J. Dewan, "Variations in the configuration of the circle of willis," *Anatomical science international*, vol. 83, pp. 96–106, 2008.

[9] M. Oumer, M. Alemayehu, and A. Muche, "Association between circle of willis and ischemic stroke: a systematic review and meta-analysis," *BMC neuroscience*, vol. 22, pp. 1–12, 2021.

[10] S. Moritz, P. Kasprzak, M. Arlt, K. Taeger, and C. Metz, "Accuracy of cerebral monitoring in detecting cerebral ischemia during carotid endarterectomy: a comparison of transcranial doppler sonography, near-infrared spectroscopy, stump pressure, and somatosensory evoked potentials," *Anesthesiology*, vol. 107, no. 4, pp. 563–569, 2007.

[11] P. V. Banga, A. Varga, *et al.*, "Incomplete circle of willis is associated with a higher incidence of neurologic events during carotid eversion endarterectomy without shunting," in *Journal of Vascular Surgery*, vol. 63, no. 6, 2016, pp. 14S–14S.

[12] L. Gibello, G. Varetto, F. Spalla, *et al.*, "Impact of the supra-aortic trunks and circle of willis patency on the neurological compensation during carotid endarterectomy," *Annals of Vascular Surgery*, vol. 60, pp. 229–235, 2019.

[13] T. Seeters, J. Hendrikse, G. Biessels, B. Velthuis, W. Mali, L. Kappelle, and Y. Graaf, "Completeness of the circle of willis and risk of ischemic stroke in patients without cerebrovascular disease." *Neuroradiology*, vol. 57, no. 12, 2015.

[14] N. Juchler, S. Schilling, P. Bijlenga, V. Kurtcuoglu, and S. Hirsch, "Shape trumps size: image-based morphological analysis reveals that the 3d shape discriminates intracranial aneurysm disease status better than aneurysm size," *Frontiers in Neurology*, vol. 13, p. 809391, 2022.

[15] N. Juchler, S. Schilling, P. Bijlenga, S. Morel, D. Rüfenacht, V. Kurtcuoglu, and S. Hirsch, "Shape irregularity of the intracranial aneurysm lumen exhibits diagnostic value," *Acta neurochirurgica*, vol. 162, pp. 2261–2270, 2020.

[16] K. Yang, F. Musio, Y. Ma, *et al.*, "Benchmarking the cow with the topcow challenge: Topology-aware anatomical segmentation of the circle of willis for cta and mra," *ArXiv*, pp. arXiv–2312, 2024.

[17] R. Nader, F. Autrusseau, V. L'allinec, and R. Bourcier, "Building a synthetic vascular model: Evaluation in an intracranial aneurysms detection scenario," *IEEE Transactions on Medical Imaging*, 2024.

[18] M. Frid-Adar, E. Klang, M. Amitai, J. Goldberger, and H. Greenspan, "Synthetic data augmentation using gan for improved liver lesion classification," in *2018 IEEE 15th international symposium on biomedical imaging (ISBI 2018)*. IEEE, 2018, pp. 289–293.

[19] G. Van Tulder and M. de Bruijne, "Why does synthesized data improve multi-sequence classification?" in *Medical Image Computing and Computer-Assisted Intervention–MICCAI 2015, Munich, Germany, Octo. 5-9, 2015*. Springer, 2015, pp. 531–538.

[20] F. Isensee, J. Petersen, S. A. Kohl, P. F. Jäger, and K. H. Maier-Hein, "nnU-Net: Breaking the spell on successful medical image segmentation," *arXiv preprint arXiv:1904.08128*, vol. 1(1-8), 2019.

[21] N. Schimke and J. Hale, "Quickshear defacing for neuroimages." *HealthSec*, vol. 11, p. 11, 2011.

[22] D. Kaltenecker, R. Al-Maskari, Negwer, *et al.*, "Virtual reality-empowered deep-learning analysis of brain cells," *Nature Methods*, pp. 1–10, 2024.

[23] R. Nader, V. l'Allinec, R. Bourcier, and F. Autrusseau, "Synthetic vascular models: Application to bifurcation classification and aneurysm detection," in *Intl. Conf. on Pattern Recog.*, 2024, pp. 63–77.